






Unconventional spin dynamics in the noncollinear phase of a ferrimagnet

D. M. Krichevsky ^{1,2,3} N. A. Gusev ^{2,3} D. O. Ignatyeva ^{2,3,4} A. V. Prisyazhnyuk,³ E. Yu. Semuk,³ S. N. Polulyakh ³ V. N. Berzhansky ³ A. K. Zvezdin,^{2,5} and V. I. Belotelov^{2,3,4}

¹*Moscow Institute of Physics and Technology (MIPT), 141700 Dolgoprudny, Russia*

²*Russian Quantum Center, 121353 Moscow, Russia*

³*Physics and Technology Institute, Vernadsky Crimean Federal University, 295007 Simferopol, Crimea*

⁴*Photonic and Quantum Technologies School, Lomonosov Moscow State University, 119991 Moscow, Russia*

⁵*Prokhorov General Physics Institute of the Russian Academy of Sciences, 119991 Moscow, Russia*



(Received 9 January 2023; accepted 20 October 2023; published 28 November 2023; corrected 14 December 2023)

Ferrimagnets possess collinear and noncollinear magnetic phases. Here we identify a crucial influence of the magnetic phase on the excited spin modes. The spin dynamics is launched in a rare-earth iron garnet film by femtosecond laser pulses. The noncollinearity cardinally changes the behavior of spin mode frequencies: the high-frequency one becomes highly sensitive to the external magnetic field while the low-frequency one gets almost field insensitive and even drops with the field growth near the transition to the collinear phase. Near the magnetization compensation point the frequencies of these modes get close to equality.

DOI: [10.1103/PhysRevB.108.174442](https://doi.org/10.1103/PhysRevB.108.174442)

I. INTRODUCTION

Ultrafast magnetic phenomena driven by femtosecond light pulses are emerging topics of modern material science. The growth in the number of studies in this field is stimulated by technological demands and fundamental puzzles ranging from ultrafast all-optical data storage [1–5] and spin transport [6,7] to quantum computing [8,9].

Ferrimagnets are unique among ordered magnetic materials as they combine properties of both ferro- and antiferromagnets. Being composed of several antiferromagnetically coupled magnetic ion sublattices, these materials sustain low-frequency (LF) ferromagnetic (FM) mode and high-frequency (HF), so-called “exchange” mode [10]. The latter is not attainable by gigahertz conventional microwave stimuli and can be excited by femtosecond laser pulses due to either thermal or optomagnonic effects [11]. Ultrafast spin dynamics along with ultrafast switching, domain-wall motion, spin waves, and skyrmion formation were extensively studied in ferrimagnetic metals, such as GdFeCo [5,12–17] and CoGd [18,19]. In contrast to metals and alloys, insulating oxides are almost lossless at optical frequencies. It makes them perfect materials for essential applications such as all-optical nonthermal magnetic recording [1,2], spintronics [20], and control of spin waves in all-dielectric nanostructures [21].

Another important feature of ferrimagnets is the possibility for full compensation of their sublattice magnetic moments which takes place at some temperature T_M called the magnetization compensation point. In the H - T phase diagram of a ferrimagnet two main phases are possible: collinear and noncollinear phases [22–25]. The collinear phase is accompanied with collinear alignment of magnetizations of both sublattices along the external magnetic field. The noncollinear phase is characterized by canting of sublattice magnetizations combined with a net magnetization slant to the external magnetic field.

Previous experiments on excitation of spin dynamics in rare-earth iron garnets (RIGs) by femtosecond laser pulses were primarily concerned with the magnetic states in the collinear phase [10,26–30] and the kind of magnetic phase was not identified. An optical excitation of the exchange resonance between rare-earth and transition metal sublattices far from the compensation point was studied in [10] for an in-plane configuration of an external magnetic field. The results were found to be in agreement with the conventional Kaplan-Kittel theory [31,32] which describes the exchange mode far from T_M . In [29,33] a comprehensive experimental study of RIGs in an in-plane magnetic field was made in a wide temperature range including magnetization compensation point, and both an exchange and FM resonances were investigated. Nevertheless, magnetic phases were not identified and corresponding features of spin dynamics were not observed. As a result, a simplified description of the mode frequencies behavior in terms of ferromagnetic resonance and Kaplan-Kittel theories satisfied the experimental data.

Importantly, the role of the magnetic phase on spin dynamics was not discussed previously and, in particular, the noncollinear phase was not addressed in this aspect. At the same time, nowadays, the room-temperature noncollinear phase, actively studied in various magnetic materials [34–36], is a potential candidate for chiral spin textures based magnetic nonvolatile memory [37], spintronic devices [38], and even qubits for quantum computing. Hence, the understanding of spin dynamics in this phase is of urgent fundamental and practical demand.

In the current work we confront the magnetic phase of a ferrimagnet with its ultrafast spin dynamics and demonstrate a crucial role of the phase state in the character of spin oscillations. Spin dynamics in the noncollinear phase of RIGs is studied comprehensively. We scrutinize magnetic phase transitions in the material via magneto-optical measurements and distinguish the temperature-dependent features of the spin

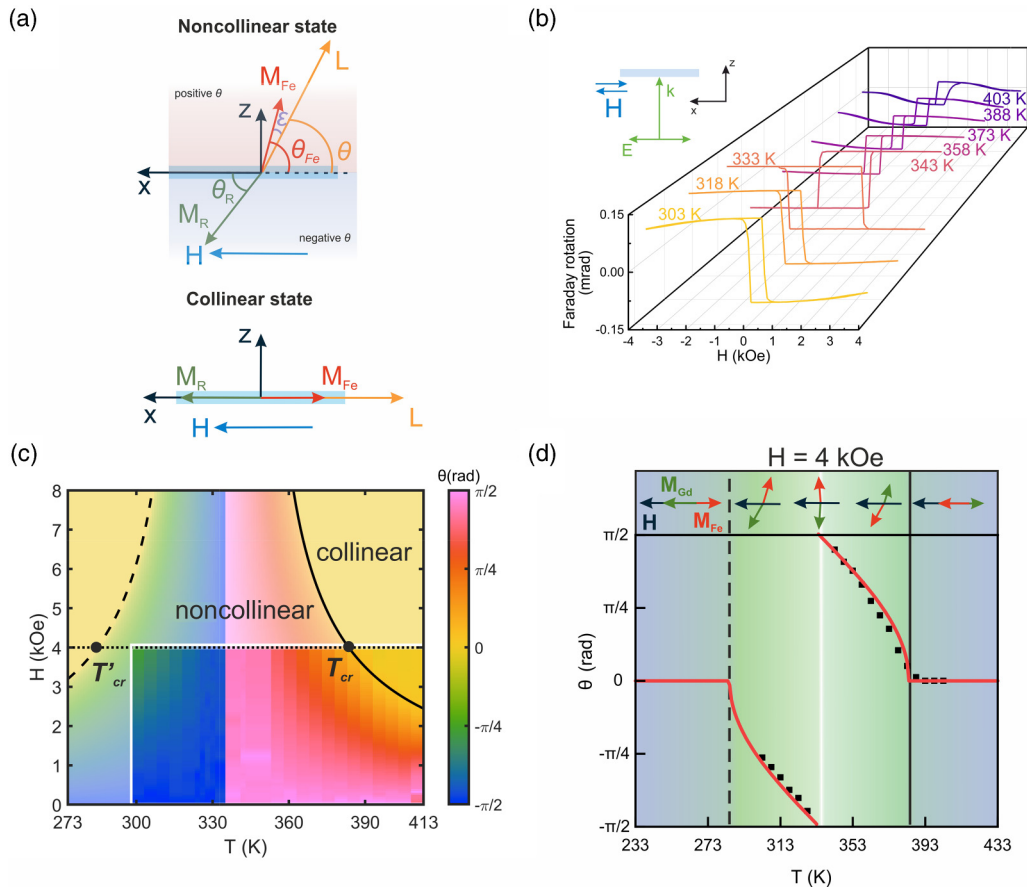


FIG. 1. (a) Configuration of the magnetic sublattices of the sample in the noncollinear and collinear phases. (b) The hysteresis loops in the in-plane magnetic field for different temperatures (inset shows experimental configuration). (c) Experimental (bright) and theoretical (blurred) phase diagrams of the RIG film. Black curves (dashed and continuous) represent phase transition boundaries between noncollinear and collinear phases. The experimental part is separated from the theoretical one by a white frame. The dotted straight line represents the slice at 4 kOe made for (d). (d) Temperature dependence of θ for the applied in-plane 4 kOe magnetic field. Black points represent experimental data, whereas the red line is the theoretical approximation (see Supplemental Material, Sec. III). The arrows show sublattice magnetization vectors orientation with respect to external magnetic field for collinear (blue filling), noncollinear (green filling), and compensated (white line) states. Vertical (dashed and continuous) lines represent boundaries between noncollinear and collinear phases.

modes by the magneto-optical pump-probe technique. Ultimately, in the noncollinear state, magnetic field dependent spin dynamics of the HF mode and inverse behavior of the LF mode were observed, which is in sharp contrast to conventional theories of ferrimagnets. The experimental results are well described by the quasi-antiferromagnetic theoretical approach.

II. RESULTS AND DISCUSSION

A. Magnetic phases

Unique magnetic properties of a RIG are governed by its complex crystal structure. Fe^{3+} ions occupy sites in tetrahedral and octahedral sublattices of the cubic unit cell, with the total magnetization of the Fe^{3+} ions in the tetrahedral positions being greater than in the octahedral ones. An uncompensated magnetic moment of Fe^{3+} ions gives rise to net magnetization \mathbf{M}_{Fe} , which is antiparallelly ordered to magnetization \mathbf{M}_R of rare-earth elements occupying the third (dodecahedral) sublattice. Due to a huge exchange field between Fe^{3+} ions in tetrahedral and oc-

tahedral sublattices they can be treated as a single one with magnetization \mathbf{M}_{Fe} in this case. Spins of the rare-earth sublattice are ordered by an exchange field produced by iron ions. The existence of T_M is mainly due to a strong temperature dependance of $M_R(T)$, while M_{Fe} is hardly affected [22–24,39,40].

The magnetization state of a RIG film can be defined using the sublattice magnetizations \mathbf{M}_{Fe} and \mathbf{M}_R forming Néel vector $\mathbf{L} = \mathbf{M}_{Fe} - \mathbf{M}_R$ and magnetization vector $\mathbf{M} = \mathbf{M}_{Fe} + \mathbf{M}_R$ [Fig. 1(a)]. The elevation angle $\theta = \frac{\theta_{Fe} - \theta_R}{2}$ characterizes the deviation of the Néel vector from the film plane, while the angle $\varepsilon = \frac{\theta_{Fe} + \theta_R}{2}$ characterizes a canting of the sublattices magnetization from a collinear antiparallel orientation. Here θ_{Fe} and θ_R are the angles between the film plane and \mathbf{M}_{Fe} and \mathbf{M}_R , respectively: $\theta > 0$ for vectors in the upper half-space of the $x - z$ plane ($z > 0$) and $\theta < 0$ for the bottom half-space ($z < 0$) [see Fig. 1(a)]. Therefore angles $\theta_{Fe,R}$ and $\theta \in [-\frac{\pi}{2}; \frac{\pi}{2}]$. Within the theoretical approach, we considered ε to be small and, based on this assumption, obtained the Lagrange function of the system and the Euler-Lagrange equations in terms of the angles of the Néel vector \mathbf{L} . Such an

approach is called the quasi-antiferromagnetic approximation [22,41] and, along with the sigma model and its modifications [17,42–44], can be used to analyze some of the two-sublattice magnetic systems. Wherein, in statics $\mathbf{M}_{\text{Fe,R}}$ always lie in the plane formed by the magnetic field and anisotropy axis (see Supplemental Material, Sec. II [45]).

Here we investigate a 2.2- μm -thick RIG film with Gd rare-earth ions $(\text{Bi}_{0.6}\text{Gd}_{2.4})(\text{Fe}_{4.28}\text{Ga}_{0.57}\text{Ge}_{0.15})\text{O}_{12}$. The film was epitaxially grown on (111) $(\text{CaGd})_3(\text{GaZrMg})_5\text{O}_{12}$ substrate and has a uniaxial magnetic anisotropy with the axis perpendicular to the film. The Faraday rotation angle at a wavelength of 515 nm is 4.54 $^\circ/\mu\text{m}$.

We consider the case when the external magnetic field is in-plane and perpendicular to the anisotropy axis. The analysis of the system's potential energy minimum reveals that in this case two magnetic phases are possible, depending on the temperature and external magnetic field: collinear and noncollinear phases (see Supplemental Material, Sec. III [45]). In the collinear phase the sublattice magnetic moments are antiparallel ($\varepsilon = 0$) and vectors \mathbf{M} and \mathbf{L} are aligned with the in-plane external magnetic field \mathbf{H} ($\theta = 0$). The noncollinear phase provides the deflection of vectors \mathbf{M} and \mathbf{L} from \mathbf{H} ($\theta \neq 0$). This deflection is accompanied by noncollinearity of the sublattices magnetic moment ($\varepsilon \neq 0$). The border between two phases is determined by the condition $m = m_{\text{cr}}$ (see Supplemental Material, Sec. III [45]). Here m is a difference between sublattice magnetizations $m = M_{\text{Fe}}(T) - M_{\text{R}}(T)$, while m_{cr} is a kind of critical magnetization defined by

$$m_{\text{cr}} = \chi_{\perp} H + \frac{2K}{H}, \quad (1)$$

where $\chi_{\perp} = \frac{(M_{\text{Fe}} + M_{\text{R}})^2}{4\Lambda M_{\text{Fe}} M_{\text{R}}} \sim \frac{1}{\Lambda}$ is magnetic susceptibility (see Supplemental Material, Sec. III [45]), Λ is an exchange parameter between Fe and rare-earth sublattices, and $K = K_{\text{Fe}} + K_{\text{R}}$, where K_{Fe} and K_{R} are anisotropy constants of each sublattice (numerical values are given in Supplemental Material, Sec. I [45]). The collinear phase exists for $|m| > m_{\text{cr}}$ and the noncollinear one establishes if $|m| < m_{\text{cr}}$. Thus, a second type of phase transition from noncollinear to collinear phases occurs at $m = m_{\text{cr}}$. This transition is directly related to the critical temperature $T_{\text{cr}}(H)$ at which $m = m_{\text{cr}}$.

To experimentally determine the magnetic phase diagram $\theta(T, H)$ we measured the magneto-optical hysteresis loops at various temperatures. Some of the loops are presented in Fig. 1(b). The experiment was carried out in an almost in-plane external magnetic field of an electromagnet (the field's tilt angle was around 1 $^\circ$). Linearly polarized (\mathbf{E} of light is directed along \mathbf{H}) normally incident 515-nm laser pulses were utilized for polarization rotation measurements. The pulses were generated by a tunable parametric amplifier (Avesta PARUS) pumped by a 1-kHz Yb regenerative amplifier (Avesta TETA). The spot size of the beam on the sample surface was $\sim 40 \mu\text{m}$, which is much smaller than the domain size under zero applied magnetic field. The sample was heated by a Peltier element electrically controlled with current stabilization. Therefore, the measured Faraday rotation angle was proportional to the out-of-plane component of the sample gyration vector. Since the gyration in RIG is mostly provided by Fe^{3+} ions [46], the observed Faraday rotation conforms to

$(\mathbf{M}_{\text{Fe}})_z$. Furthermore, since the tilt between Fe and Gd sublattices given by angle ε is small (see Supplemental Material, Sec. II [45]), such measurement provides deflection of the Néel vector ($\theta \approx \theta_{\text{Fe}}$). At zero magnetic field \mathbf{M}_{Fe} is directed normally to the surface ($\theta_{\text{Fe}} = \pi/2$) due to the uniaxial magnetic anisotropy. A magnetic field applied in-plane deflects \mathbf{M}_{Fe} from the normal. Consequently, θ is found as follows:

$$\theta(H, T) \approx \theta_{\text{Fe}}(H, T) = \sin^{-1} \left(\frac{\text{FR}(H, T)}{|\text{FR}(0, T)|} \right), \quad (2)$$

where $\text{FR}(H, T)$ and $\text{FR}(0, T)$ are angles of the Faraday rotation (FR) under applied magnetic field H and zero magnetic field, correspondingly. To determine the phase diagram $\theta(H, T)$ only one branch of the hysteresis loops $\text{FR}(H, T)$ can be considered. In our case we used the one corresponding to a decrease of the external magnetic field from $H_{\text{max}} = 4$ kOe to 0.

The experimentally measured magnetic phase diagram $\theta(T, H)$ and its cross section at $H = 4$ kOe are given in Figs. 1(c) and 1(d), respectively [additional cross sections of Fig. 1(c) are presented in Supplemental Material, Sec. V [45]]. A distinct jump of derivative $\partial\theta/\partial T$ takes place at $m = m_{\text{cr}}$ [solid black curve in Fig. 1(c)], e.g., at $T_{\text{cr}} \sim 383$ K for $H = 4$ kOe [Fig. 1(d)], indicating the second kind of phase transition. The other phase transition of the second kind appears for smaller temperatures when $m < 0$ and $|m| = m_{\text{cr}}$ [dashed black curve in Fig. 1(c)] which corresponds to $T'_{\text{cr}} \sim 284$ K at $H = 4$ kOe [Fig. 1(d)]. For a fixed H the noncollinear phase ($\theta \neq 0$) appears for the temperature interval $T'_{\text{cr}}(H) < T < T_{\text{cr}}(H)$. This temperature range decreases for larger magnetic fields [Fig. 1(c)] which is due to the increasing Zeeman energy of the sample. Notably, in the noncollinear phase, theory predicts bistability of the system due to the degeneracy of the $+\theta$ and $-\theta$ states (see Supplemental Material, Sec. III, Fig. S3 [45]). However, in our experiments a small out-of-plane magnetic field component exists which lifts this degeneracy and selects the direction of M_z projection parallel to this small out-of-plane field component. Hence \mathbf{L} flips while crossing the magnetization compensation temperature T_{M} due to a change of sign of m at T_{M} , which indicates that for the studied sample $T_{\text{M}} = 336$ K.

B. Spin dynamics peculiarities

Ultrafast spin dynamics in the sample was excited by 787-nm circularly polarized 250-fs laser pump pulses incident at $\sim 10^\circ$ of polar angle and observed by the FR of the femtosecond laser probe pulses at 515 nm delayed with respect to the pump pulse in the configuration shown in Fig. 2(a). The pulses were produced by the same laser system used for the static magneto-optical measurements. The pump and probe pulses were focused on the sample to a 100- μm (fluence of 30 mJ/cm^2) and a 40- μm (fluence of 0.3 mJ/cm^2) spot, correspondingly. The pump-probe experiment was conducted in a wide temperature range which allowed us to observe features of the noncollinear states below and above T_{M} . Moreover, we resolved the spin dynamics at the phase transition ($T_{\text{cr}} = 383$ K at $H = 4$ kOe) and in the collinear phase, for larger temperatures [Fig. 2(b)]. Figures 2(b) and 2(c) demonstrate the

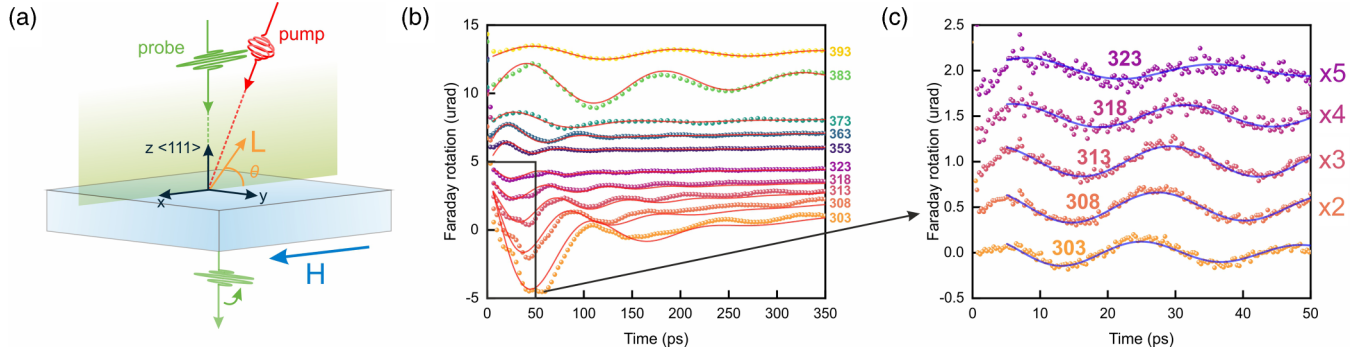


FIG. 2. Configuration of the pump-probe experiment (a). Ultrafast magnetization dynamics represented by the probe Faraday transients in the range of 350 ps for different temperatures from 303 K (below T_M) to 393 K (above T_M): (b) general view for the range up to 350 fs and (c) zoomed view for the range of 50 ps demonstrating the HF mode in detail. The data in (c) are presented after subtracting the LF mode. The amplitude of the oscillations in (c) for 308–323 K are scaled (the scale factor is presented on the right side of the figure). Fitted curves from Eqs. (3) and (4) are colored red and blue in (b) and (c), respectively.

dynamics of the Néel vector in terms of the time-resolved Faraday polarization rotation (TRFR) at $H = 4$ kOe. Two kinds of oscillations are clearly observed: LF ones at the timescale up to 350 ps [Fig. 2(b)] and HF ones at the timescale of 50 ps [Fig. 2(b) and the zoomed view in Fig. 2(c)]. Notably, the HF component in the TRFR signal was not observed for the temperatures above T_M . To obtain frequencies of the observed oscillations, a fitting procedure using a nonlinear least-squares method was carried out. As the first step, to obtain the parameters of the LF mode, we utilized the following function:

$$F_{LF}(t) = A_0 + A_1 \exp(-\lambda_1 t) + A_2 \sin(2\pi f_2 + \varphi_2) \times \exp(-\lambda_2 t). \quad (3)$$

In Eq. (3) f_2 is the frequency of the LF mode. Next, we subtracted $F_{LF}(t)$ at timescales 0–50 ps from the experimental data to obtain Fig. 2(c). The subtracted data were fitted with the function presented below:

$$F_{HF}(t) = A_3 \sin(2\pi f_3 + \varphi_3) \exp(-\lambda_3 t). \quad (4)$$

The frequency f_3 in Eq. (4) represents the HF mode. Data on the frequencies of these modes collected from gauged TRFR signals were then compared to theoretical values [Figs. 3(a) and 3(b)].

Theoretical analysis of the spin dynamics in the current ferromagnetic system is performed based on the Euler-Lagrange equations of motion (see Supplemental Material, Sec. II [45]). In our calculations we assumed that the gyromagnetic ratio of Fe and Gd ions is equal ($\gamma_{Fe} = \gamma_{Gd} = \gamma$) [47–50]. In the noncollinear phase ($|m| < m_{cr}$) the mode frequencies are given by (see Supplemental Material, Sec. IV)

$$\omega_{HF,LF} = \left(\Omega_1^2 + \Omega_2^2 + \omega_0^2 \pm \sqrt{(\Omega_1^2 + \Omega_2^2)^2 + 2\omega_0^2 \Omega_2^2} \right)^{1/2}, \quad (5)$$

where $\Omega_1^2 = \frac{\omega_H^2}{2} - \omega_H \omega_{KK} \cos \theta$, $\Omega_2^2 = \frac{1}{2}(2\omega_H \cos \theta - \omega_{KK})^2$, $\omega_H = \gamma H$, $\omega_{KK} = \gamma \frac{|m|}{\chi_{\perp}} = \gamma \Lambda |m|$, and $\omega_0 = \gamma \sqrt{2K/\chi_{\perp}}$. In Eq. (5) the sign “+” corresponds to the HF mode while the sign “−” corresponds to the LF one [inset in Fig. 3(a)]. Frequencies of the modes for the collinear state are presented in the Supplemental Material, Sec. IV [45]. The frequencies

calculated using Eq. (5) [solid curves in Figs. 3(a) and 3(b)] agree well with the experimental findings [dots in Figs. 3(a) and 3(b)].

Actually, the experimental and calculation data shown in Fig. 3 along with Eq. (5) represent the special features of this work. The features of the HF and LF modes in the noncollinear state differ drastically from those in the collinear phase far from T_M and should be discussed in detail. Let us start from the HF mode. Conventionally, it is described as the Kaplan-Kittel exchange mode, whose frequency is nearly unaffected by the external magnetic field and is primarily influenced by the exchange magnetic field [10,26,29]: $\omega_{HF} = \omega_{KK} = \gamma \Lambda |m|$. However, in the noncollinear state the situation dramatically changes: the Kaplan-Kittel formula is no longer valid and when temperature approaches the compensation point ω_{HF} goes to some minimum value given by $\omega_{HF}(T_M) = \gamma \sqrt{\frac{2K}{\chi_{\perp}} + H^2}$. Consequently, in the noncollinear phase the HF mode frequency does depend on the external magnetic field and in the vicinity of T_M and in relatively low magnetic fields ω_{HF} depends on H quadratically. This provides an important and convenient tool for its control that was previously unavailable in the collinear states far from T_M .

The behavior of the LF mode is nearly the opposite. Typically, the frequency of the LF mode depends on the applied magnetic field in the collinear state and is well described by the Kittel formula: $\omega_{LF} = \gamma \sqrt{H(H - \frac{2K}{|m|} + 4\pi |m|)}$ (e.g., see Ref. [29]). However, in the noncollinear state this turns upside-down: the q-FM mode becomes hardly sensitive to the magnetic field, as shown in Fig. 3(a) by blue symbols. Near the compensation point Eq. (5) gives for the LF mode $\omega_{LF}(T_M) = \gamma \sqrt{\frac{2K}{\chi_{\perp}}}$.

Moreover, our study shows [Fig. 3(b)] that near the compensation point f_{HF} and f_{LF} become close to each other: f_{HF} decreases and f_{LF} increases for the temperature increase towards T_M so that both modes have extremums at this temperature. There is only a small frequency gap at T_M : $\Delta f = \frac{\gamma}{2\pi} (\sqrt{\frac{2K}{\chi_{\perp}} + H^2} - \sqrt{\frac{2K}{\chi_{\perp}}})$, which can be controlled by an external magnetic field. Please note that at the temperatures far from T_M , the frequencies of the two modes have several orders

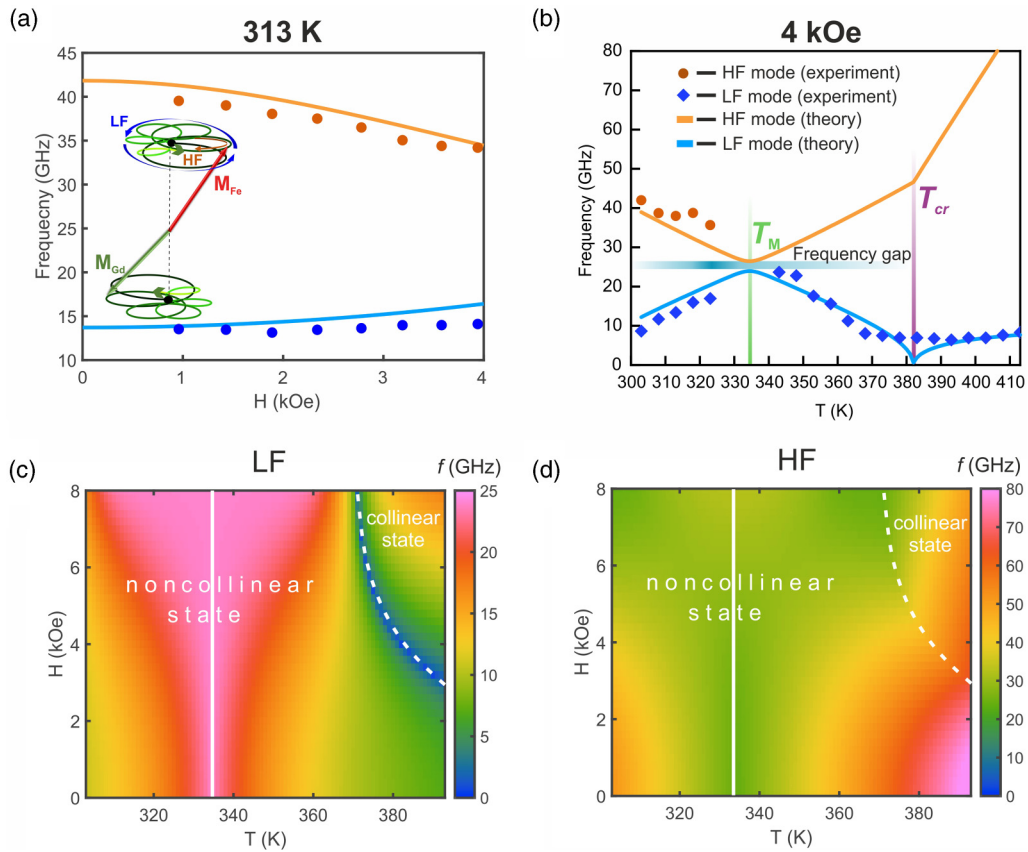


FIG. 3. (a),(b) Experimentally found frequencies of the LF (blue dots) and HF (brown dots) modes compared to theoretical curves calculated from Eq. (3): (a) versus magnetic field at $T = 313$ K and (b) versus temperature for $H = 4$ kOe. The inset in (a) shows the complex trajectory of \mathbf{M}_{Fe} and \mathbf{M}_R vectors during laser-induced simultaneous excitation of the LF and HF modes. The trajectory is shown for the time interval equal to one period of the q-FM mode. Six periods of the HF mode are seen. Color of the trajectory curve denotes the temporal coordinate, so that the dynamics starts at the black point and proceeds to the light-green color. (c),(d) Calculated oscillation frequencies of the HF (c) and LF modes (d) as a function of external magnetic field and temperature. White dashed lines at (c) and (d) indicate the boundary of phase transition between noncollinear and collinear phases.

difference. For example, frequencies of 3 and 410 GHz were observed for the FM and exchange modes for the films far from the compensation point at similar experimental conditions [26].

We broadened the view of mode frequencies behavior and calculated the frequencies of the LF and HF modes for different values of the external magnetic field and temperature using Eq. (3) [Figs. 3(c) and 3(d)]. A boundary between the collinear and noncollinear phases are shown in Figs. 3(c) and 3(d) by a dashed white line. A peculiar nonmonotonous dependence of f_{LF} on the magnetic field is observed in the noncollinear phase near the phase transition temperature T_{cr} : it decreases with the increase of the magnetic field [Fig. 3(c)], which is in high contrast with what happens in the collinear phase and in the ferromagnetic materials. Notably, the theory predicts that at T_{cr} , f_{LF} tends to zero [Figs. 3(b) and 3(c)], which indicates a soft mode character [25].

III. CONCLUSION

To conclude, in this study, we identify an importance of the magnetic phase of a ferrimagnet for its ultrafast spin behavior. A rare-earth iron garnet near magnetization compensation

temperature was considered. We demonstrated several crucial peculiarities of spin dynamics in a noncollinear state that contrast sharply with the usually observed spin dynamics of the exchange and ferromagnetic modes in a collinear state far from the compensation point. In particular, when the temperature approaches the compensation point, the frequencies of the HF and LF modes behave oppositely: the former decreases, while the latter one grows. The situation changes after crossing the compensation point for higher temperatures. We also discovered that the transition from the noncollinear phase to the collinear one is accompanied with softening of the LF mode which leads to its frequency minimization. In contrast to the conventional case of the collinear phase in the noncollinear one, the behavior turns upside-down: The HF mode gets a field-dependent character, while the LF mode becomes almost field independent, which is in agreement with our theoretical predictions based on quasi-antiferromagnetic approximation of Euler-Lagrange equations of motion. The described methodology allows temperature control of the magnetization states of RIG for magnonic and spintronic devices. The approach described in the current study is universal and can be applied for RIG with various rare-earth ions as well as for other ferrimagnets with uniaxial anisotropy.

ACKNOWLEDGMENTS

The experimental part of this work was financially supported by the Ministry of Science and Higher Education of the Russian Federation, Megagrant Project No. 075-15-2022-

1108. Theoretical part of this work was financially supported by the Russian Science Foundation, Project No. 23-62-10024. We also thank N. E. Khokhlov for help in preparation of the experimental setup for the pump-probe experiments.

-
- [1] A. Stupakiewicz, K. Szerenos, D. Afanasiev, A. Kirilyuk, and A. V. Kimel, Ultrafast nonthermal photo-magnetic recording in a transparent medium, *Nature (London)* **542**, 71 (2017).
- [2] A. Stupakiewicz, C. S. Davies, K. Szerenos, D. Afanasiev, K. S. Rabinovich, A. V. Boris, A. Caviglia, A. V. Kimel, and A. Kirilyuk, Ultrafast phononic switching of magnetization, *Nat. Phys.* **17**, 489 (2021).
- [3] A. V. Kimel and M. Li, Writing magnetic memory with ultrashort light pulses, *Nat. Rev. Mater.* **4**, 189 (2019).
- [4] J. Gorchon, C.-H. Lambert, Y. Yang, A. Pattabi, R. B. Wilson, S. Salahuddin, and J. Bokor, Single shot ultrafast all optical magnetization switching of ferromagnetic Co/Pt multilayers, *Appl. Phys. Lett.* **111**, 042401 (2017).
- [5] C. D. Stanciu, A. Tsukamoto, A. V. Kimel, F. Hansteen, A. Kirilyuk, A. Itoh, and T. Rasing, Subpicosecond magnetization reversal across ferrimagnetic compensation points, *Phys. Rev. Lett.* **99**, 217204 (2007).
- [6] J. R. Hortensius, D. Afanasiev, M. Matthiesen, R. Leenders, R. Citro, A. V. Kimel, R. V. Mikhaylovskiy, B. A. Ivanov, and A. D. Caviglia, Coherent spin-wave transport in an antiferromagnet, *Nat. Phys.* **17**, 1001 (2021).
- [7] T. Kampfrath, M. Battiato, P. Maldonado, G. Eilers, J. Nötzold, S. Mährlein, V. Zbarsky, F. Freimuth, Y. Mokrousov, S. Blügel *et al.*, Terahertz spin current pulses controlled by magnetic heterostructures, *Nat. Nanotechnol.* **8**, 256 (2013).
- [8] J. Zou, S. Bosco, B. Pal, S. S. P. Parkin, J. Klinovaja, and D. Loss, Quantum computing on magnetic racetracks with flying domain wall qubits, *Phys. Rev. Res.* **5**, 033166 (2023).
- [9] H. Y. Yuan, Y. Cao, A. Kamra, R. A. Duine, and P. Yan, Quantum magnonics: When magnon spintronics meets quantum information science, *Phys. Rep.* **965**, 1 (2022).
- [10] S. Parchenko, T. Satoh, I. Yoshimine, F. Stobiecki, A. Maziewski, and A. Stupakiewicz, Non-thermal optical excitation of terahertz-spin precession in a magneto-optical insulator, *Appl. Phys. Lett.* **108**, 032404 (2016).
- [11] A. Kirilyuk, A. V. Kimel, and T. Rasing, Ultrafast optical manipulation of magnetic order, *Rev. Mod. Phys.* **82**, 2731 (2010).
- [12] I. Radu, K. Vahaplar, C. Stamm, T. Kachel, N. Pontius, H. A. Dürr, T. A. Ostler, J. Barker, R. F. L. Evans, R. W. Chantrell *et al.*, Transient ferromagnetic-like state mediating ultrafast reversal of antiferromagnetically coupled spins, *Nature (London)* **472**, 205 (2011).
- [13] J. Becker, A. Tsukamoto, A. Kirilyuk, J. C. Maan, T. Rasing, P. C. M. Christianen, and A. V. Kimel, Ultrafast magnetism of a ferrimagnet across the spin-flop transition in high magnetic fields, *Phys. Rev. Lett.* **118**, 117203 (2017).
- [14] K. Vahaplar, A. M. Kalashnikova, A. V. Kimel, D. Hinzke, U. Nowak, R. Chantrell, A. Tsukamoto, A. Itoh, A. Kirilyuk, and T. Rasing, Ultrafast path for optical magnetization reversal via a strongly nonequilibrium state, *Phys. Rev. Lett.* **103**, 117201 (2009).
- [15] C. D. Stanciu, A. V. Kimel, F. Hansteen, A. Tsukamoto, A. Itoh, A. Kirilyuk, and T. Rasing, Ultrafast spin dynamics across compensation points in ferrimagnetic GdFeCo: The role of angular momentum compensation, *Phys. Rev. B* **73**, 220402(R) (2006).
- [16] K. Vahaplar, A. M. Kalashnikova, A. V. Kimel, S. Gerlach, D. Hinzke, U. Nowak, R. Chantrell, A. Tsukamoto, A. Itoh, A. Kirilyuk *et al.*, All-optical magnetization reversal by circularly polarized laser pulses: Experiment and multiscale modeling, *Phys. Rev. B* **85**, 104402 (2012).
- [17] K.-J. Kim, S. K. Kim, Y. Hirata, S.-H. Oh, T. Tono, D.-H. Kim, T. Okuno, W. S. Ham, S. Kim, G. Go *et al.*, Fast domain wall motion in the vicinity of the angular momentum compensation temperature of ferrimagnets, *Nat. Mater.* **16**, 1187 (2017).
- [18] M. Binder, A. Weber, O. Mosendz, G. Woltersdorf, M. Izquierdo, I. Neudecker, J. R. Dahn, T. D. Hatchard, J.-U. Thiele, C. H. Back *et al.*, Magnetization dynamics of the ferrimagnet CoGd near the compensation of magnetization and angular momentum, *Phys. Rev. B* **74**, 134404 (2006).
- [19] L. Caretta, M. Mann, F. Büttner, K. Ueda, B. Pfau, C. M. Günther, P. Helsing, A. Churikova, C. Klose, M. Schneider *et al.*, Fast current-driven domain walls and small skyrmions in a compensated ferrimagnet, *Nat. Nanotechnol.* **13**, 1154 (2018).
- [20] M. V. Logunov, S. S. Safonov, A. S. Fedorov, A. A. Danilova, N. V. Moiseev, A. R. Safin, S. A. Nikitov, and A. Kirilyuk, Domain wall motion across magnetic and spin compensation points in magnetic garnets, *Phys. Rev. Appl.* **15**, 064024 (2021).
- [21] A. I. Chernov, M. A. Kozhaev, D. O. Ignatyeva, E. N. Beginin, A. V. Sadovnikov, A. A. Voronov, D. Karki, M. Levy, and V. I. Belotelov, All-dielectric nanophotonics enables tunable excitation of the exchange spin waves, *Nano Lett.* **20**, 5259 (2020).
- [22] M. D. Davydova, K. A. Zvezdin, A. V. Kimel, and A. K. Zvezdin, Ultrafast spin dynamics in ferrimagnets with compensation point, *J. Phys.: Condens. Matter* **32**, 01LT01 (2020).
- [23] M. D. Davydova, K. A. Zvezdin, J. Becker, A. V. Kimel, and A. K. Zvezdin, *H-T* phase diagram of rare-earth-transition-metal alloys in the vicinity of the compensation point, *Phys. Rev. B* **100**, 064409 (2019).
- [24] Ch. K. Sabdenov, M. D. Davydova, K. A. Zvezdin, D. I. Gorbunov, I. S. Tereshina, A. V. Andreev, and A. K. Zvezdin, Magnetic-field induced phase transitions in intermetallic rare-earth ferrimagnets with a compensation point, *Low Temp. Phys.* **43**, 551 (2017).
- [25] A. K. Zvezdin and A. F. Popkov, Magnetic-resonance in ferromagnets with compensation point, *Solid State Phys.* **16**, 1082 (1974).
- [26] S. Parchenko, A. Stupakiewicz, I. Yoshimine, T. Satoh, and A. Maziewski, Wide frequencies range of spin excitations in a rare-earth Bi-doped iron garnet with a giant Faraday rotation, *Appl. Phys. Lett.* **103**, 172402 (2013).
- [27] A. H. M. Reid, A. V. Kimel, A. Kirilyuk, J. F. Gregg, and Th. Rasing, Optical excitation of a forbidden magnetic resonance

- mode in a doped lutetium-iron-garnet film via the inverse Faraday effect, *Phys. Rev. Lett.* **105**, 107402 (2010).
- [28] M. Deb, P. Molho, B. Barbara, and J. Y. Bigot, Controlling laser-induced magnetization reversal dynamics in a rare-earth iron garnet across the magnetization compensation point, *Phys. Rev. B* **97**, 134419 (2018).
- [29] M. Deb, P. Molho, B. Barbara, and J. Y. Bigot, Temperature and magnetic field dependence of rare-earth \leftrightarrow iron exchange resonance mode in a magnetic oxide studied with femtosecond magneto-optical Kerr effect, *Phys. Rev. B* **94**, 054422 (2016).
- [30] T. G. H. Blank, K. A. Grishunin, E. A. Mashkovich, M. V. Logunov, A. K. Zvezdin, and A. V. Kimel, THz-scale field-induced spin dynamics in ferrimagnetic iron garnets, *Phys. Rev. Lett.* **127**, 037203 (2021).
- [31] J. Kaplan and C. Kittel, Exchange frequency electron spin resonance in ferrites, *J. Chem. Phys.* **21**, 760 (1953).
- [32] C. Kittel, On the theory of ferromagnetic resonance absorption, *Phys. Rev.* **73**, 155 (1948).
- [33] M. Deb, P. Molho, and B. Barbara, Magnetic damping of ferromagnetic and exchange resonance modes in a ferrimagnetic insulator, *Phys. Rev. B* **105**, 014432 (2022).
- [34] R. Sahoo, L. Wollmann, S. Selle, T. Höche, B. Ernst, A. Kalache, C. Shekhar, N. Kumar, S. Chadov, C. Felser *et al.*, Compensated ferrimagnetic tetragonal Heusler thin films for antiferromagnetic spintronics, *Adv. Mater.* **28**, 8499 (2016).
- [35] V. Kumar, N. Kumar, M. Reehuis, J. Gayles, A. S. Sukhanov, A. Hoser, F. Damay, C. Shekhar, P. Adler, and C. Felser, Detection of antiskyrmions by topological Hall effect in Heusler compounds, *Phys. Rev. B* **101**, 014424 (2020).
- [36] W.-Y. Choi, W. Yoo, and M.-H. Jung, Emergence of the topological Hall effect in a tetragonal compensated ferrimagnet $\text{Mn}_{2.3}\text{Pd}_{0.7}\text{Ga}$, *NPG Asia Mater.* **13**, 79 (2021).
- [37] Y. Hirata, D.-H. Kim, S. K. Kim, D.-K. Lee, S.-H. Oh, D.-Y. Kim, T. Nishimura, T. Okuno, Y. Futakawa, H. Yoshikawa *et al.*, Vanishing skyrmion Hall effect at the angular momentum compensation temperature of a ferrimagnet, *Nat. Nanotechnol.* **14**, 232 (2019).
- [38] D. Céspedes-Berrocal, H. Damas, S. Petit-Watelot, D. Maccariello, P. Tang, A. Arriola-Córdova, P. Vallobra, Y. Xu, J.-L. Bello, E. Martin *et al.*, Current-induced spin torques on single GdFeCo magnetic layers, *Adv. Mater.* **33**, 2007047 (2021).
- [39] M. S. Lataifeh and A. Al-sharif, Magnetization measurements on some rare-earth iron garnets, *Appl. Phys. A: Mater. Sci. Process.* **61**, 415 (1995).
- [40] S. Geller, J. P. Remeika, R. C. Sherwood, H. J. Williams, and G. P. Espinosa, Magnetic study of the heavier rare-earth iron garnets, *Phys. Rev.* **137**, A1034 (1965).
- [41] A. K. Zvezdin, Dynamics of domain walls in weak ferromagnets, *Zh. Eksp. Teor. Fiz., Pis'ma Red.* **29**, 553 (1979).
- [42] B. A. Ivanov, Ultrafast spin dynamics and spintronics for ferrimagnets close to the spin compensation point (Review), *Low Temp. Phys.* **45**, 935 (2019).
- [43] B. A. Ivanov and A. L. Sukstanskii, Nonlinear magnetization waves in ferrites, *J. Exp. Theor. Phys.* **84**, 214 (1983).
- [44] B. A. Ivanov and V. E. Kireev, Macroscopic coherent tunneling in a small particle of an uncompensated antiferromagnet in a strong magnetic field, *JETP Lett.* **69**, 398 (1999).
- [45] See Supplemental Material at <http://link.aps.org/supplemental/10.1103/PhysRevB.108.174442> for magnetic properties of the sample, quasi-antiferromagnetic theoretical approach description, theoretical phase diagrams, frequencies of the spin modes, and cross sections of the phase diagram.
- [46] V. A. Zvezdin and A. K. Kotov, *Modern Magneto-optics and Magneto-optical Materials* (CRC Press, Boca Raton, FL, 1997).
- [47] A. B. Drovoskov, N. M. Kreines, A. O. Savitsky, E. A. Kravtsov, M. V. Ryabukhina, V. V. Proglyado, and V. V. Ustinov, Magnetization and ferromagnetic resonance in a Fe/Gd multilayer: Experiment and modelling, *J. Phys.: Condens. Matter* **29**, 115802 (2017).
- [48] G. F. Dionne, Molecular field and exchange constants of Gd^{3+} -substituted ferrimagnetic garnets, *J. Appl. Phys.* **42**, 2142 (1971).
- [49] S. Geprägs, A. Kehlberger, F. D. Coletta, Z. Qiu, E.-J. Guo, T. Schulz, C. Mix, S. Meyer, A. Kamra, M. Althammer *et al.*, Origin of the spin Seebeck effect in compensated ferrimagnets, *Nat. Commun.* **7**, 10452 (2016).
- [50] A. Stupakiewicz and T. Satoh, Ultrafast optomagnonics in ferrimagnetic multi-sublattice garnets, *J. Phys. Soc. Jpn.* **90**, 081008 (2021).

Correction: The second sentence of the Acknowledgments contained an error and has been remedied.